Flavor Dependence of Charged Pion Fragmentation Functions

H. Bhatt,[1] P. Bosted,[2] S. Jia,[3] W. Armstrong,[4] D. Dutta,[1] R. Ent,[5] D. Gaskell,[5] E. Kinney,[6] H. Mkrtchyan,[7] S. Ali,[8] R. Ambrose,[9] D. Androic,[10] C. Ayerbe Gayoso,[1] A. Bandari,[2] V. Berdnikov,[8] D. Bhetuwal,[1] D. Biswas,[11] M. Boer,[3] E. Brash,[12] A. Camsonne,[5] J. P. Chen,[5] J. Chen,[2] M. Chen,[13] S. Covrig,[5] M. Diefenthaler,[5] B. Duran,[3] M. Elaasar,[14] C. Elliot,[15] H. Fenker,[5] E. Fuchey,[16] J. O. Hansen,[5] F. Hauenstein,[17] T. Horn,[8] G. M. Huber,[9] M. K. Jones,[5] M. L. Kabir,[1] A. Karki,[1] B. Karki,[18] S. Kay,[9] C. Keppel,[5] V. Kumar,[9] N. Lashley-Colthirst,[11] W. B. Li,[2] D. Mack,[5] S. Malace,[5] P. Markowitz,[19] M. McCaughhan,[5] E. McClellan,[5] D. Meekins,[5] R. Michaels,[5] A. Mkrtchyan,[7] G. Niculescu,[20] I. Niculescu,[20] S. Park,[21] E. Pooser,[5] M. Rehfuss,[3] G. R. Smith,[5] H. Szumila-Vance,[5] A. S. Tadepalli,[5] V. Tadevosyan,[7] R. Trotta,[8] H. Voskanyan,[7] S. A. Wood,[5] Z. Ye,[4] C. Yero,[19] and X. Zheng[13]

(for the Hall C Collaboration)

[1]*Mississippi State University, Mississippi State, Mississippi 39762, USA*
[2]*The College of William & Mary, Williamsburg, Virginia 23185, USA*
[3]*Temple University, Philadelphia, Pennsylvania 19122, USA*
[4]*Argonne National Laboratory, Lemont, Illinois 60439, USA*
[5]*Thomas Jefferson National Accelerator Facility, Newport News, Virginia 23606, USA*
[6]*University of Colorado Boulder, Boulder, Colorado 80309, USA*
[7]*A.I. Alikhanyan National Science Laboratory (Yerevan Physics Institute), Yerevan 0036, Armenia*
[8]*Catholic University of America, Washington, DC 20064, USA*
[9]*University of Regina, Regina, Saskatchewan S4S 0A2, Canada*
[10]*University of Zagreb, Zagreb, Croatia*
[11]*Hampton University, Hampton, Virginia 23669, USA*
[12]*Christopher Newport University, Newport News, Virginia 23606, USA*
[13]*University of Virginia, Charlottesville, Virginia 22903, USA*
[14]*Southern University at New Orleans, New Orleans, Louisiana 70126, USA*
[15]*University of Tennessee, Knoxville, Tennessee 37996, USA*
[16]*University of Connecticut, Storrs, Connecticut 06269, USA*
[17]*Old Dominion University, Norfolk, Virginia 23529, USA*
[18]*Ohio University, Athens, Ohio 45701, USA*
[19]*Florida International University, University Park, Florida 33199, USA*
[20]*James Madison University, Harrisonburg, Virginia 22807, USA*
[21]*Stony Brook University, Stony Brook, New York 11794, USA*

(Dated: June 28, 2024)

We have measured the flavor dependence of multiplicities for π^+ and π^- production in semi-inclusive deep-inelastic scattering (SIDIS) on proton and deuteron targets. Using an electron beam with energies of 10.2 and 10.6 GeV at Jefferson Lab and the Hall-C spectrometers (HMS for electrons, SHMS for pions), the lepton vertex spanned the kinematic range $0.3 < x < 0.6$, $2 < Q^2 < 5$ GeV^2, and $4 < W^2 < 11$ GeV^2. The pion fractional momentum range was 0.3$< z <$0.7, and the transverse momentum range was $0 < p_T < 0.25$. Assuming factorization at low p_T and allowing for isospin breaking, we find that the results can be described by two "favored" and two "un-favored", effective low p_T fragmentation functions that are flavor-dependent. However, they converge to a common flavor-independent value at the lowest x or highest W of this experiment.

Semi-inclusive deep-inelastic lepton-nucleon scattering ($lN \rightarrow l^{'}hX$) is an excellent tool to study the quark hadronization mechanism described by the fragmentation function (FF) [1]. The FFs describe how the quarks and gluons transform into color-neutral hadrons or photons during high-energy (hard) scattering processes. Pion semi-inclusive deep-inelastic scattering (SIDIS) is one such scattering process that allows access to the FFs associated with the pions identified in the final state. Studies of FFs will prove critical for a complete understanding of the basic properties of quantum chromodynamics (QCD) as they are intrinsically linked to confinement in QCD. The FFs are the non-perturbative ingredient of the QCD factorization theorems [2] used to analyze hard scattering processes and thereby provide insight into fundamental soft QCD quantities [3]. The current knowledge of pion FFs is based on global QCD analyses [4–9] that are dominated by measurements from inclusive electron-positron (e^+e^-) annihilation into charged pions at very high energy scales. e^+e^- annihilation is a clean process to study FFs since it is independent of the parton distribution functions (PDF), however, it cannot distinguish between the light quark flavors or the quark and anti-quark FFs. Information about possible flavor dependence of the FFs is essential for a complete picture of the FFs as well as the spin structure of nucleons, in particular the transverse spin structure [10]. Further, the SIDIS experiments conducted over the last decade have also convincingly established that the colinear picture of the quark-parton model is too simple, highlighting the importance of the transverse structure of the hadrons. The flavor structure of FFs is important to understand the flavor dependence of the transverse momentum dependent (TMD) FFs [10] and the relative differences of the asymmetries observed between pions and kaons [11, 12]. Thus, SIDIS measurements provide a unique capability to study the flavor structure of FFs at an energy scale that is complementary to that of the e^+e^- annihilation.

The FFs cannot be deduced from first principles and are challenging to model as they are non-perturbative objects. Current models treat the hadronization either as a sequential emission of hadrons from colored partons with emission probability parameterized to describe experimental data, such as the Lund string model [13], or approximate it as the emission of a single hadron and an on-shell spectator quark [14]. Another recent approach uses a combination of these two methods by calculating the emission probability within a QCD-inspired spectator model instead of a parameterization [15]. As charge symmetry (CS) and isospin symmetry (IS) are fundamental properties of QCD and strong interaction processes, all of the studies use a simple quark flavor-independent (for light quarks) and isospin-independent ansatz. At the quark level, CS refers to the invariance of the QCD Hamiltonian under rotations about the 2-axis in isospin space, i.e. the interchange of up and down quarks while simultaneously interchanging protons and neutrons. As the fragmentation process is a dominantly strong interaction process, the FFs are expected to respect CS to high precision. Moreover, CS allows one to drastically reduce the number of independent FFs. Most global fits of existing data that extract FFs either assume CS and IS or find no significant violation [5, 7]. On the other hand, a recent global analysis reported a significant flavor dependence of the FFs [16], and measurements on the transverse polarization of the Λ hyperon in e^+e^- annihilations by the Belle collaboration [17] seem to indicate a significant IS violation in the corresponding FFs and pose a significant challenge to QCD. These results, and the quest for transverse momentum-dependent FFs have created an urgent need for a systematic study of the flavor dependence of FFs and their charge and isospin symmetry violation. Additionally, any flavor dependence of the FFs would have a significant impact on the test of CS in PDFs being undertaken at Jefferson Lab (JLab) [18].

One of the most important advantages of SIDIS is the ability to tag the flavor of the quark involved in the scattering process. Consequently, measuring the SIDIS process on protons and deuterons allows an independent extraction of the flavor dependence of the FFs. Additionally, the sum and difference ratio of π^+ and π^- production on hydrogen to those produced from deuterium serves as an effective test of charge and isospin symmetry. In order to exploit these advantages a new experimental program was undertaken at the upgraded JLab [18–20]. An integral part of this program, featuring measurements on both hydrogen and deuterium targets over a wide range of kinematics [18, 19], was completed in 2019. In this letter, we report the results of the tests of charge and isospin symmetry violation and flavor dependence of the unpolarized FFs extracted from this experimental program.

The p_t-integrated semi-inclusive pion electroproduction yield ($\frac{dN}{dz}$) as a function of the pion's longitudinal momentum fraction z is usually modeled as;

$$\frac{dN}{dz} \sim \sum_i e_i^2 q_i(x, Q^2) D_{q_i \to \pi}(z, Q^2) \tag{1}$$

where the quarks of flavor i with charge e_i carrying a fraction x of nucleon momentum are represented by the PDFs, $q_i(x, Q^2)$, and the spin averaged FFs by $D_{q_i \to \pi}(z, Q^2)$. As a consequence of co-linear factorization, the PDFs are independent of z and FFs are independent of x, but depend on the virtuality scale, or 4-momentum transferred square, Q^2, via a logarithmic evolution [2, 21]. We define the measured multiplicities for π^+, π^- production from hydrogen (p) and deuterium (d) targets, $M_{p/d}^{\pi^\pm}(x, Q^2, z)$, as the ratio of the respective SIDIS cross section to the DIS cross section (see Eq. (1) in the online Supplementary Material). At leading order, assuming CS and no difference in transverse momentum (p_t) dependence for the measured multiplicities, we can write two simple ratios, as shown in Eqs. 2 and 3.

$$R_1(z) = \frac{M_d^{\pi^+}(z) + M_d^{\pi^-}(z)}{M_p^{\pi^+}(z) + M_p^{\pi^-}(z)} = 1 \tag{2}$$

and

$$R_2(z) = \frac{M_d^{\pi^+}(z) - M_d^{\pi^-}(z)}{M_p^{\pi^+}(z) - M_p^{\pi^-}(z)} = \frac{3\,(4u(x) + d(x))}{5\,(4u(x) - d(x))}, \tag{3}$$

where, the up(down) $u(d)$ quark PDFs are written as; $u(x) = u_v(x) + \bar{u}(x)$ and $d(x) = d_v(x) + \bar{d}(x)$, with $u_v(d_v)$ and $\bar{u}(\bar{d})$ as the valance quark and sea anti-quark contributions, respectively. Here the quark and anti-quark contributions from the sea are assumed symmetric and the strange quark contributions are neglected. For measurements made in the valence region ($x > 0.3$) where the contributions from the sea quarks can be neglected the difference ratio reduces to $R_2(z) \sim \frac{3}{5}$, making both ratios independent of z and p_T. Thereby, these two ratios constitute an excellent test of CS and IS within the co-linear factorization formalism.

Most global analyses to extract PDFs assume IS and CS in the PDFs which reduces the number of independent PDFs by half. If we assume no charge/iso-spin symmetry violation (CSV/ISV) in the PDFs but allow for non-zero CVS/ISV in the FFs, the multiplicity $M_{p/d}^{\pi^\pm}(x, Q^2, z)$ for each target (H/D) and charged pion type can be written in terms of two favored FFs, $D_{u\pi^+}(z)$, $D_{d\pi^-}(z)$, and two un-favored FFs, $D_{d\pi^+}(z)$, $D_{u\pi^-}(z)$, respectively (see

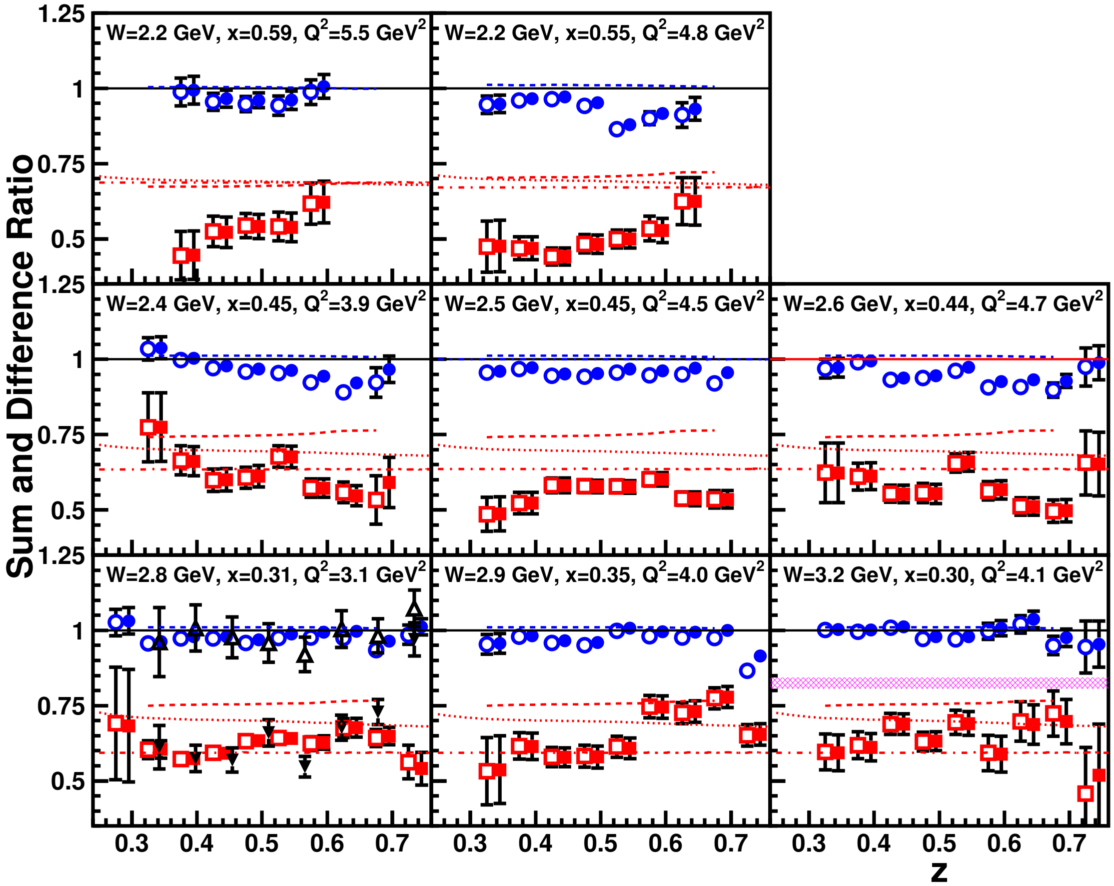

FIG. 1. The sum ratios (circles) and difference ratios (squares) $R_1(z)$ and $R_2(z)$ as a function of z for eight kinematic settings ordered in increasing values of W when going from left to right with similar values of x for each row. The closed (open) symbols are without (with) subtraction of the diffractive ρ^0 contributions. The solid (dotted) lines are the predictions for any model with isospin symmetry for the sum (difference) ratio. The dashed curves use the FF from the MAPS [9] collaboration and the dot-dashed curves are the FFs from the DSS [5, 7] fits. The open (closed) triangles in the bottom-left panel show the sum (difference) ratio obtained from the previous JLab 6 GeV experiment [21]. Although the previous results were at a similar x =0.32, the W and Q^2 were at a significantly lower value of 2.4 GeV and 2.3 GeV^2 respectively. The magenta hatched band in the bottom-right panel shows the 2.2% systematic uncertainty of these ratios.

Eq. (2) in the supplementary material). Any difference between the two favored and the two un-favored FFs is an indication of CSV in the FFs. The amount of CSV in the favored and un-favored FFs can be quantified in terms of two asymmetries defined as:

$$A_{\rm f}(z) = \frac{D_{u\pi^+} - D_{d\pi^-}}{D_{u\pi^+} + D_{d\pi^-}}, \quad A_{\rm uf}(z) = \frac{D_{d\pi^+} - D_{u\pi^-}}{D_{d\pi^+} + D_{u\pi^-}} \qquad (4)$$

Most current global analyses to extract FFs predict these asymmetries to be either exactly or effectively zero.

We have measured the four p_T integrated multiplicities for the electroproduction of $\pi^\pm$ from hydrogen and deuterium targets. These multiplicities along with the PDFs from a global fit by the Jefferson Lab Angular Momentum collaboration (JAM) [8], were used to extract the four FFs. We have assumed an identical p_T dependence for the $\pi^\pm$ multiplicities from hydrogen and deuterium, integrated over p_T with an average of $< p_T > \;=\; 0.1$ GeV/c. The CSV of the FFs was quantified in terms of the two asymmetries in Eq. 4. The experiment was carried out in the Fall of 2018 and the Spring of 2019, in Hall C at JLab. The experiment used the quasi-continuous wave electron beam with beam energies of 10.2 and 10.6 GeV and beam currents ranging from 2 μA to 70 μA. Additional details of the experiment are described in Sec. 1 of the Supplementary Material. The experimental yields from the ^{1}H and ^{2}H targets were obtained by integrating the charge-normalized coincidence events over a phase space defined by restricting the bounds of the reconstructed momentum and angular acceptances and constraining the missing mass of the residual system, M_X, to be above the resonance region ($M_X > 1.6$ GeV/c^2). The yields were integrated over azimuthal angle ϕ and p_T The backgrounds from the target's aluminum windows and accidental coincidences were subtracted. This normalized SIDIS pion electroproduction yield was corrected for all known inefficiencies of the two spectrometers such as the detector efficiencies (97%–99%), trigger efficiency (98%-99%), tracking efficiencies, computer and electronic live times (94%–99%). The corrected yields were binned in z for the 8 different kinematic settings where the x ranged from 0.3 to 0.6, Q^2 ranged from 3.1 to 5.5 GeV^2 and the center-of-mass energy, W, ranged from 2.2 to 3.2 GeV. The table of kinematic settings is shown in the supplementary material.

A Monte Carlo simulation [22] of the SIDIS process was performed with the factorized form shown in Eq. 1. The CTEQ5 next-to-leading-order (NLO) PDFs were used to parametrize $q(x;Q^2)$ [23] along with a parametrization of the FF from global fits of SIDIS data [24]. Additional details about the models used in the simulation can be found in Refs. [25, 26]. The Monte Carlo package was used to determine the radiative corrections by simulating the radiative tails for the SIDIS pion electroproduction and accounting for the radiative tails from exclusive pion electroproduction off protons and neutrons that fall within the experimental acceptance. The Monte Carlo package was also used to correct for pion decay and the contributions from electroproduction of ρ^0 mesons and $\Delta(1232)$ resonances. The Monte Carlo yields were integrated over the same phase space as the measured yields.

The corrected experimental yields for the 8 different settings were used along with the Monte Carlo yield and the model cross section to obtain the four multiplicities, $M^{\pi^\pm}_{p/d}(x, Q^2, z)$. The 2.8% systematic uncertainties of the multiplicities is described and listed in Table Table II of the Supplementary Materials. The four multiplicities were used to form the two ratios $R_1(z)$ and $R_2(z)$, and also used to obtain four FFs ($D_{u\pi^+}(z), D_{d\pi^-}(z)$ and $D_{u\pi^-}(z), D_{d\pi^+}(z)$) by simultaneously solving a system of four equations (Eq. (2) in the supplementary material).

The extracted sum and difference ratios are shown as a function of z in Fig. 1 along with the statistical uncertainties, the 2.2% systematic uncertainty is shown by the magenta band in the bottom-right panel. The estimation of the systematic uncertainties are described in the Supplementary Material. The negligible difference between the open and closed symbols shows that the diffractive ρ^0 contribution to the pion yield has very little impact on these ratios. The solid (dotted) lines are expectations for models with isospin symmetry for the sum (difference) ratio. The dot-dashed and dashed curves use the FFs from the global fits by the DSS [5, 7] and MAPS [9] collaborations respectively. At the highest W (3.2 GeV) the two ratios are remarkably independent of z over the entire range ($z = 0.3$ - 0.7) and are also consistent with the magnitude predicted by the global fits to existing data. In other words, the results agree with the charge symmetry expectation. The sum ratio R_1 slowly but steadily deviates from the charge symmetry expectation with increasing x or decreasing W, both in terms of the z independence and the magnitude. Similarly, the difference ratio also shows increasingly large deviations from the charge symmetry expectation with increasing x (decreasing W). These deviations may indicate the importance of higher twist contributions to the SIDIS cross sections at low W (large x). These results also indicate that even for the limited range of p_T covered in this experiment, charge symmetry seems to be valid for $x < 0.4$ or $W > 3$ GeV. Moreover, the sum/difference ratio from the previous JLab 6 GeV experiment [21] agrees remarkably well with the current results. The older ratios were obtained at the same $x = 0.32$, but at significantly lower W and Q^2 of 2.4 GeV and 2.3 GeV^2 respectively. This seems to indicate that x is the more relevant variable for tests of charge/isospin symmetry.

The four extracted FFs are shown as a function of W^2 in Fig. 8 of the Supplementary Materials, for 8 different z bins ranging from $z = 0.325$ to 0.675. Note that our data confirm that the p_T dependence for the $\pi^\pm$ multiplicities from hydrogen and deuterium are identical within the small p_T range covered. The two favored and two un-favored FFs were used to form the favored and un-favored asymmetries as defined in Eq. 4 and are shown in Fig. 2. Only the statistical uncertainties are shown, the uncertainty due to the systematic uncertainty of the FFs are not shown as they are negligible compared to the statistical uncertainties (see Supplementary Material for details). The favored asymmetries are essentially zero within the experimental uncertainties over the entire range of z and x. At the highest W or lowest x, they are consistent with the expectations of the DSS [7] fits but not the fits of Peng and Ma [16].

The statistical uncertainties of the un-favored asymmetries are significantly larger than those for the favored asymmetries. Even within these large uncertainties, the un-favored asymmetries are consistent with zero at the lowest x (highest W). These results are a direct experimental confirmation of charge/isospin symmetry for both the favored and un-favored FFs at the lowest x (highest W) kinematics. As noted in Fig. 1, for the lowest x (highest W) kinematics the sum and difference ratios are also consistent with the charge symmetry expectation. These results confirm that for x <0.4 or $W > 3$ GeV the FFs are flavor-independent and the SIDIS process obeys charge/isospin symmetry within experimental uncertainties. The results also show a more complex fragmentation process at higher x (lower W), with possible contributions from higher-order corrections.

The poor statistics in the un-favored down quark fragmentation channel drives the large uncertainty in the un-favored fragmentation function asymmetry. Even in an isoscalar target, up quark scattering is a majority of the DIS cross section due to a larger electromagnetic coupling, and the poor statistics are exacerbated for SIDIS by the un-favored fragmentation configuration. Lack-

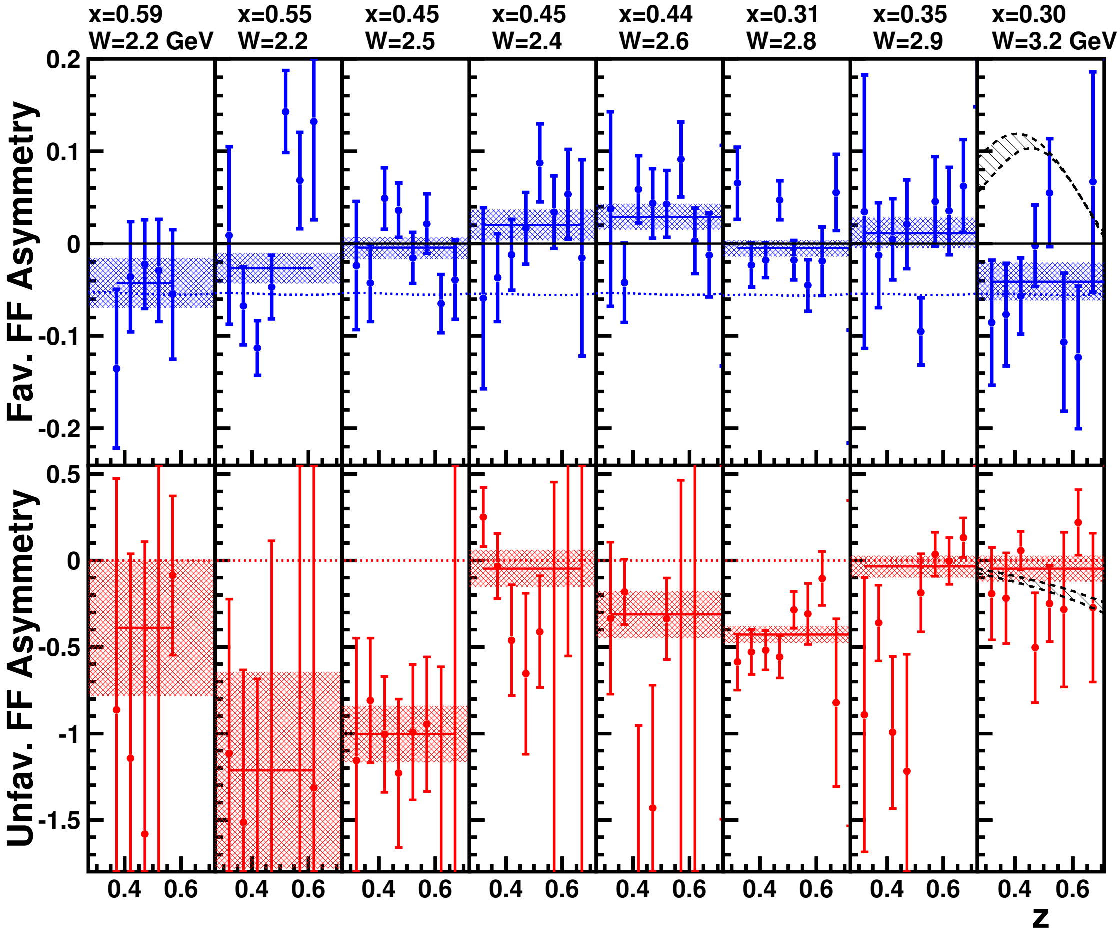

FIG. 2. The z dependence of the charge/isospin symmetry violating asymmetry of the favored FFs (top panels) and un-favored FFs (bottom panels), extracted from the measured charged pion multiplicities on hydrogen and deuterium targets. Horizontally, the panels are ordered in decreasing values of x (increasing W). The blue (red) solid lines are constant value fits for each panel of the favored (un-favored) asymmetry with the shaded bands indicating the statistical uncertainty of the fit. Assuming charge symmetry the two asymmetries should be zero as indicated by the black solid line (top panels). The black hatched band in the last panels is the asymmetry and its uncertainty from the global fit by Peng and Ma [16], while the dotted lines are from the DSS global fits [5, 7].

ing a free neutron target, tagging the spectator (A-1) system isolates hard scattering on the neutron. Future high-luminosity measurements with a spectator tagging of a proton or ^{3}He (using a D or ^{4}He target respectively) can significantly improve the uncertainties for un-favored down quark fragmentation.

In summary, we have measured the $\pi^\pm$ multiplicities from SIDIS on hydrogen and deuterium targets over a wide range of kinematics. The sum and difference ratios of the four multiplicities satisfy charge/isospin symmetry for $x < 0.4$ or $W > 3.0$ GeV. The multiplicities were also used to quantify the flavor dependence of FFs and they confirm the flavor independence of both the favored and un-favored FFs for $x < 0.4$ or $W > 3.0$ GeV. The results also indicate that higher-twist corrections are important for high x (low W). The inclusion of the data reported here into future global fits of PDFs and FFs should provide further detailed insight into the fragmentation process. These results also suggest that the forthcoming extraction of CSV in PDFs from the deuteron data will not be impacted by possible CSV in the FFs. The spectator tagging technique pioneered at JLab could be used in future experiments to access almost free neutron targets to improve the precision of the unfavoured FFs and their CSV.

This work was funded in part by the U.S. Department of Energy, including contract AC05-06OR23177 under which Jefferson Science Associates, LLC operates Thomas Jefferson National Accelerator Facility, and by the U.S. National Science Foundation and the Natural

Sciences and Engineering Research Council of Canada. We wish to thank the staff of Jefferson Lab for their vital support throughout the experiment. We are also grateful to all granting agencies providing funding support to authors throughout this project.

[1] R. D. Field and R. P. Feynman, Phys. Rev. D **15**, 2590 (1977).
[2] J. C. Collins, D. E. Soper, and G. Sterman, Adv. Ser. Direct. High Energy Phy. **5**, 1 (1988).
[3] S. Albino, Rev. Mod. Phys. **82**, 2489 (2010).
[4] M. Hirai, S. Kumano, T. Nagai, and K. Sudoh, Phys. Rev. D **75**, 094009 (2007).
[5] D. deFlorian, R. Sassot, and M. Stratmann, Phys. Rev. D **75**, 114010 (2007).
[6] S. Albino, B. Kniehl, and G. Kramer, Nucl. Phys. B **803**, 42 (2008).
[7] D. deFlorian, R. Sassot, M. Epele, R. J. Hernández-Pinto, and M. Stratmann, Phys. Rev. D **91**, 014035 (2015).
[8] E. Moffat, W. Melnitchouk, T. C. Rogers, and N. Sato, Phys. Rev. D **104**, 016015 (2021).
[9] A. Bacchetta, V. Bertone, C. Bissolotti, G. Bozzi, M. Cerutti, F. Piacenza, M. Radici, and A. Signori, J. of High Eng. Phys. **10**, 127 (2022).
[10] A. Signori, A. Bacchetta, M. Radici, and G. Schnell, J. of High Eng. Phy. **11**, 194 (2013).
[11] A. Airapetian *et al.*, Phys. Rev. Lett. **103**, 152002 (2009).
[12] C. Adolph *et al.*, Phys. Lett. B **744**, 250 (2015).
[13] B. Andersson, G. Gustafson, G. Ingelman, and T. Sjöstrand, Phys. Reports **97**, 31 (1983).
[14] P. Mulders and R. Tangerman, Nucl. Phys. B **461**, 197 (1996).
[15] T. Ito, Phys. Rev. D **80**, 074008 (2009).
[16] Q. Peng and B.-Q. Ma, Phys. Rev. C **107**, 055202 (2023).
[17] Y. Guan *et al.*, Phys. Rev. Lett. **122**, 042001 (2019).
[18] K. Hafidi, D. Gaskell, D. Dutta, *et al.*, Jefferson Lab experiment E12-09-002.
[19] H. Mkrtchyan, P. Bosted, R. Ent, E. Kinney, *et al.*, Jefferson Lab experiment E12-09-017.
[20] H. Avakian *et al.*, The CLAS12 collaboration, Run groups A and B.
[21] T. Navasardyan *et al.*, Phys. Rev. Lett. **98**, 022001 (2007).
[22] `https://hallcweb.jlab.org/simc/`,.
[23] H. L. Lai *et al.*, Phys. Rev. D **55**, 1280 (1997).
[24] P. Bosted, Private communication.
[25] H. Bhatt, PhD Thesis, Mississippi State University, 2023.
[26] S. Jia, PhD Thesis, Temple University, 2022.

Supplementary Material for Flavor Dependence of Charged Pion Fragmentation Functions

I. THE EXPERIMENT

The experiment was carried out in Hall C at Jefferson Lab using a quasi-continuous wave electron beam with energies of 10.2 to 10.6 GeV and beam currents ranging from 2 μA to 70 μA. The beam energy was measured with $< 0.05\%$ relative uncertainty from the bend angle of the beam as it traversed a set of magnets with precisely known field integrals. The total accumulated beam charge was determined using a set of resonant-cavity based beam-current monitors and a parametric transformer as gain monitor. The relative uncertainty of the accumulated beam charge was $\approx 0.5\%$, after correcting for zero-offsets and saturation effects measured using beam current scans on a solid carbon target. The beam was rastered at ≈ 25 kHz over a 2×2 mm^2 square pattern to minimize density reduction in the target due to localized beam heating.

The main production targets were a 10-cm-long (726 mg/cm^2) liquid hydrogen target and a 10-cm-long (1690 mg/cm^2) liquid deuterium target. Two aluminum foils placed 10-cm apart were used to determine the background from the aluminum entrance (≈ 14 mg/cm^2) and exit (≈ 19 mg/cm^2) end caps of the cryogenic target cells. A small reduction in density due to localized beam heating was determined to be -0.023%/μA for the liquid hydrogen target and -0.027%/μA for the liquid deuterium target.

Scattered electrons were detected in the High Momentum Spectrometer [1] in coincidence with charged pions detected in the Super High Momentum Spectrometer [2]. The angle and momentum of the electron arm (13 - 49 deg., 1 - 6 GeV/c) and the hadron arm (6 - 30 deg., 2 - 7 GeV/c) were chosen to map the region between $0.2 \leq x \leq 0.6$ and $0.3 \leq z \leq 0.7$, where x is the fraction of nucleon momentum carried by the struck quark and z is the pion's longitudinal momentum fraction. The angle, θ_{pq}, between the electron three-momentum transfer, $\vec{q}$ and the hadron momentum, was chosen to cover a range in pion transverse momentum p_T up to 0.25 GeV/c. The kinematics of the experiment are listed in Table I.

The detector packages in the two spectrometers are similar, and they included four segmented planes of plastic scintillators (except for the last plane in the SHMS which used quartz bars) that were used to form the trigger in order to read out the time and amplitude signals from all of the detectors. To ensure nearly 100% efficiency for the triggers, signals from any three out of the four planes in each spectrometer were required. The time resolution of each plane was about 0.5 nsec, resulting in an accuracy of typically 0.3 nsec when all four planes were combined. Two drift chambers, each containing six planes of wires oriented at 0° and ±60° with respect to the horizontal, provided position and direction (track) information at the spectrometer focal plane with a resolution of <250 μm. The track information was used to reconstruct the momentum and the angle of the particle at the target (reaction vertex). After many improvements to the tracking software, the tracking efficiency in the HMS was determined to be over 99.7% throughout the experiment as shown in Fig. 1 (left). For the SHMS, the tracking efficiency varied between 99.5% at low currents to 98% at the highest beam currents. The rate dependence of the tracking efficiency was slightly different between the Spring 2018 and Fall 2019 run periods, as shown in Fig. 1 (right).

In the HMS (the electron spectrometer), a threshold gas Cherenkov detector and a segmented Pb-glass calorimeter [3] were used for electron identification. A constant efficiency of 98% was estimated for the Cherenkov detector in the HMS, as shown in Fig. 2 (left). The efficiency of the HMS calorimeter was ∼99% throughout the experiment as shown in Fig. 2 (right).

The pions in the SHMS (the hadron spectrometer) were identified using the electron-hadron coincidence time, the heavy-gas (C_4F_8O at less than 1 atm. pressure) threshold Cherenkov detector, the aerogel Cherenkov detector [4] and a segmented Pb-glass calorimeter [3]. The pion identification efficiency of the aerogel Cherenkov varied between 94% for low momentum pions to 97% for the highest momentum pions as shown in Fig. 3 (left). The SHMS calorimeter efficiency was ∼ 96% as shown in Fig. 3 (right) The heavy-gas threshold Cherenkov detector had an inefficient region near the center of the detector. The events from this inefficient region were removed from the analysis using a geometric cut as shown in Fig. 4 (left). The efficiency of the heavy-gas Cherenkov detector above the pion threshold, after removing events from the inefficient region, is shown in Fig. 4 (right).

In addition, the radio-frequency (RF) time information provided for each beam bucket along with electron-hadron coincidence time was also used for particle identification. The purity of the pion sample was determined using the RF timing information with and without constraints from the heavy-gas Cherenkov, as shown in Fig. 5 (left) for the positive pions. Events with positive pion momenta above 2.8 GeV/c have significant kaon contamination when not suppressed by the constraint from the heavy-gas Cherenkov detector. This contamination was negligible for negative pions. In this analysis the heavy-gas Cherenkov was used to suppress the kaons therefore a pion purity of 1.0 was assumed. The difference in the extracted multiplicity, with kaon rejection using the heavy-gas Cherenkov or with a correction to the pion purity when not using the heavy-gas Cherenkov, was used to de-

TABLE I. The eight kinematic settings where data were collected on both hydrogen and deuterium targets.

Ebeam	E'	θ_e	Q^2	W	x	p_π	θ_π
(GeV)	(GeV/c)	(deg)	(GeV^2)	(GeV)		(GeV/c)	(deg)
10.2	5.240	18.51	5.5	2.2	0.59	2.219, 2.713, 3.208	17.75
10.6	5.971	15.75	4.8	2.2	0.55	1.838, 2.299, 2.761, 3.223	18.55
10.6	5.971	14.24	3.9	2.4	0.45	1.838, 2.299, 2.761, 3.223	17.04
10.6	5.240	16.30	4.5	2.5	0.45	2.525, 3.363, 5.04	8-26
10.6	4.945	17.26	4.7	2.6	0.44	2.241, 2.804, 3.366, 3.928	14.16
10.6	5.240	13.50	3.1	2.8	0.31	1.956, 2.575, 3.433, 4.79	8-30
10.6	4.483	16.64	4.0	2.9	0.35	2.428, 3.037, 3.646, 4.234	11.61
10.6	3.307	19.70	4.1	3.2	0.30	2.645, 3.393, 4.531, 6.786	8-22

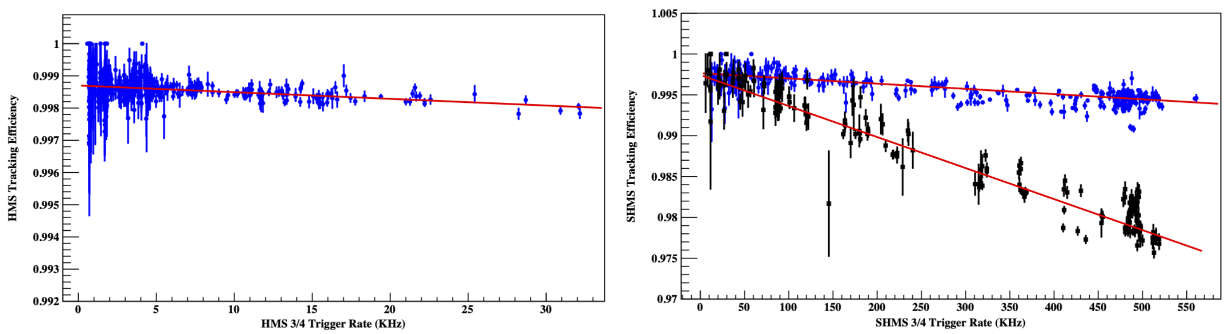

FIG. 1. The tracking efficiency of the HMS (left) and SHMS (right) drift chambers as a function of the 3/4 trigger rate. The rate dependence of the efficiency is fit to a first order polynomial. For the HMS the χ^2 per degree of freedom is 1.2. For the SHMS the χ^2 per degree of freedom is 7.9 for the Spring 2018 (black squared) and 1.2 for the Fall 2019 (blue circles) run periods. The tracking efficiency corrections were applied run-by-run and only the statistical uncertainties are shown.

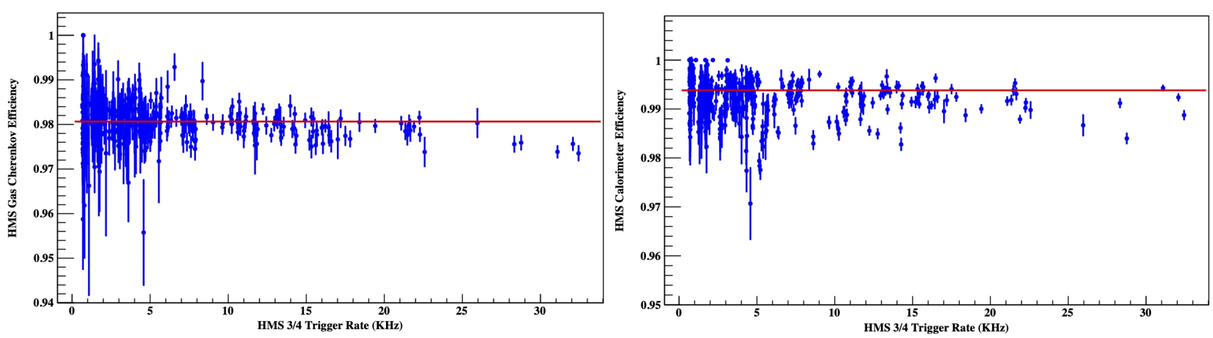

FIG. 2. The HMS gas Cherenkov efficiency (left) and the HMS calorimeter efficiency (right) as a function of HMS 3/4 trigger rate. The solid lines show the constant value fits for each, with a χ^2 per degree-of-freedom of 1.7 and 9.9, respectively. For the HMS gas Cherenkov, a constant value of 0.98 was used as the correction factor, while a constant value of 0.994 was used for the calorimeter. Only the statistical uncertainties are shown.

termine the systematic uncertainty due to kaon contamination of the pion sample. This difference was negligible for negative pions. The efficiency of the RF constraint as a function of SHMS momentum is shown in Fig. 5 (right) for π^+ (black squares) and π^- (red circles).

The electron-pion coincidence events were recorded in 1-hour-long runs via a data acquisition system operated using the CEBAF Online Data Acquisition (CODA) software package [5]. The accidental backgrounds were subtracted by sampling the accidental events corresponding to several adjacent beam buckets on either side of the true coincident events. Prescaled singles (inclusive) electron and proton events were simultaneously recorded for systematic studies. The corrections for particle energy loss through the spectrometers were determined to be better than 1%.

Data collected on the two aluminum foil targets were used to subtract the events from the aluminum walls of the cryogenic target cell. The background from π^0 production and subsequent decay to two photons and eventually converting to electron-positron pairs was determined to be negligible based on representative data

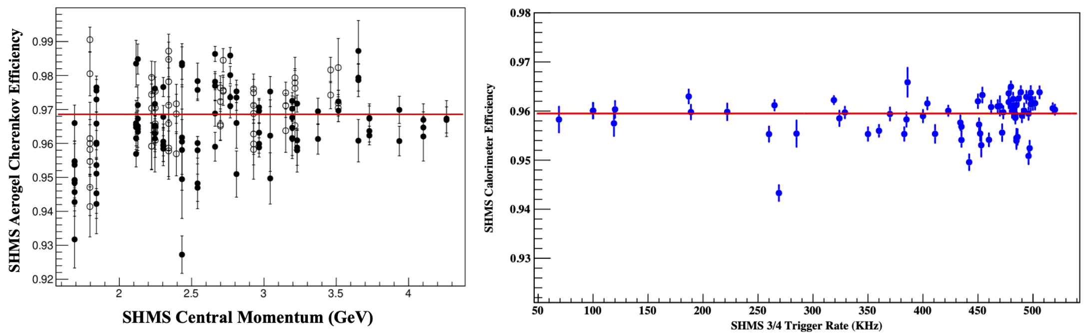

FIG. 3. (left) The pion identification efficiency of the SHMS aerogel detector as a function of the pion momentum for π^+ (solid) and π^- (open). (right) The SHMS calorimeter efficiency as a function of 3/4 trigger rate (π^+). The solid lines are constant values fits that were used as the efficiency corrections. Only the statistical uncertainties are shown.

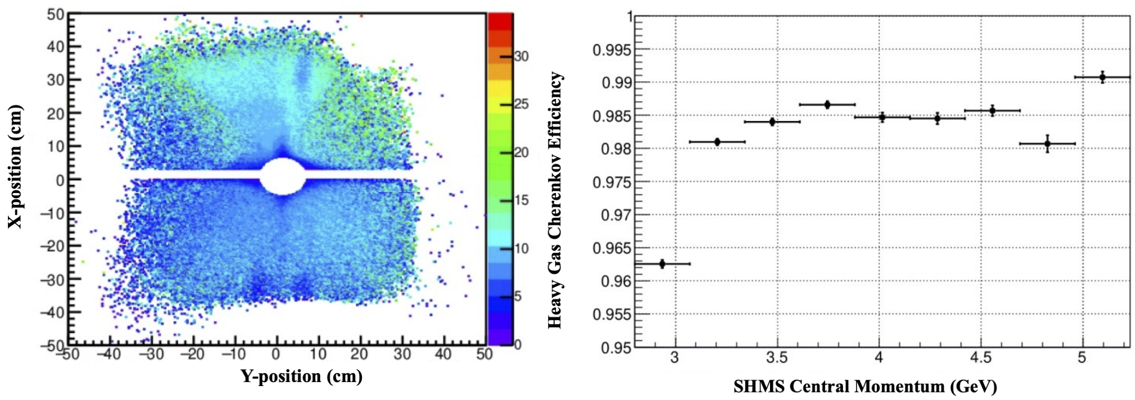

FIG. 4. The x-position vs. y-position of hits on the heavy-gas Cherenkov detector, showing the inefficient region of the Cherenkov detector that was removed from the analysis (left). The efficiency of the heavy-gas Cherenkov detector as a function of the SHMS momentum (right).

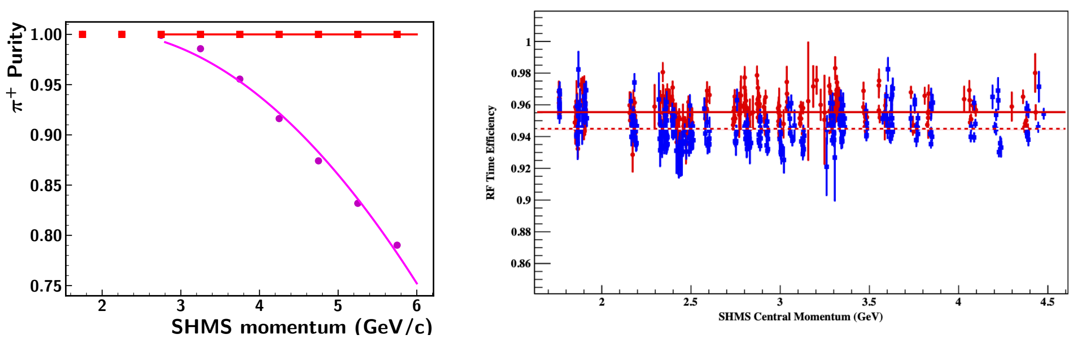

FIG. 5. (left) The purity of the pion sample with (red squares) and without (magenta circles) constraints from the heavy-gas Cherenkov as a function of the pion momentum. (right) The RF time efficiency of the π^+ (blue squares) and π^- (red circles) as a function of SHMS central momentum. The lines are the constant value fits for π^+ (dotted) and π^- (solid) with χ^2 per degree of freedom 3.86 and 6.21 respectively. A constant value of 0.95 was used as the RF time efficiency throughout the experiment. Only the statistical uncertainties are shown.

collected by detecting positrons in the HMS. The total live-time (product of the electronic and computer live-times) of the data acquisition (DAQ) system was measured using a special trigger called an Electronic Dead Time Monitor (EDTM). The EDTM consists of a known fixed-frequency trigger, deliberately chosen to be low rate (10 Hz in this experiment) such that it does not block the real trigger. The ratio of the recorded to the expected EDTM triggers was used as the total live-time of the DAQ. The total live time plotted as a function of the

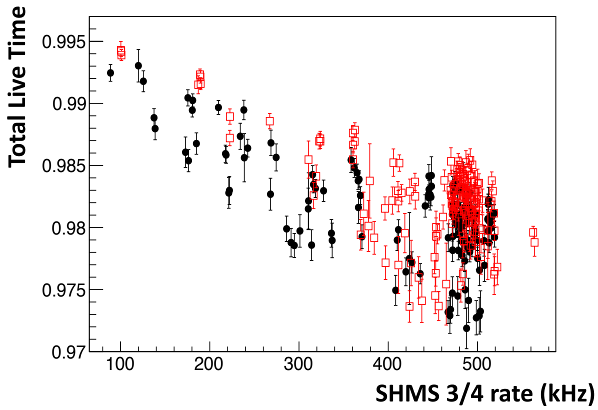

FIG. 6. The total live time of the π^+ (red open squares) and π^- (black circles) events as a function of the trigger rate in the SHMS which was the hadron spectrometer. Only the statistical uncertainties are shown.

hadron trigger rate in the SHMS spectrometer is shown in Fig. 6.

II. DATA ANALYSIS

The charge-normalized and background subtracted coincidence yield on the ^{1}H and ^{2}H targets were obtained by integrating the experimental phase space, including azimuthal angle ϕ and p_T. This normalized SIDIS pion electroproduction yield was corrected for the live-time and all the inefficiencies listed earlier and binned in z. The corrected yield along with yields from the Monte Carlo simulation were used to extract the multiplicity, defined as the ratio of the SIDIS cross section to the DIS cross section for each target (p/d) and charged pion type given by:

$$M^{\pi^\pm}_{p/d}(x, Q^2, z) = \frac{d\sigma_{ee'\pi X}}{d\sigma_{ee'X}} = \frac{\sum_i e_i^2 q_i^{p/d}(x) D_{q_i\to\pi^\pm}(z)}{\sum_i e_i^2 q_i^{p/d}(x)}, \tag{1}$$

The four multiplicities at different values of z are shown as a function of W^2 in Fig. 7. The four multiplicities show the expected z dependence (i.e decreasing monotonically with increasing z). They also show an increase in the slope of the W^2 dependence as the z increases.

Assuming charge symmetry for PDFs but not for the fragmentation functions (FFs), the multiplicity $M^{\pi^\pm}_{p/d}(x, Q^2, z)$ can be expanded in terms of the up and down quark content of the two targets as given by Eq. 2 below;

$$\begin{aligned}
&M^{\pi^+}_p(x, Q^2, z) = \\
&\quad \frac{D_{u\pi^+}(z)\left[4u(x)+\bar{d}(x)\right] + D_{d\pi^+}(z)\left[d(x)+4\bar{u}(x)\right]}{4u(x)+4\bar{u}(x)+d(x)+\bar{d}(x)} \\
&M^{\pi^-}_p(x, Q^2, z) = \\
&\quad \frac{D_{d\pi^-}(z)\left[4\bar{u}(x)+d(x)\right] + D_{u\pi^-}(z)\left[\bar{d}(x)+4u(x)\right]}{4u(x)+4\bar{u}(x)+d(x)+\bar{d}(x)} \\
&M^{\pi^+}_d(x, Q^2, z) = \\
&\quad \frac{D_{u\pi^+}(z)[4u(x)+4d(x)+\bar{u}(x)+\bar{d}(x)]}{5[u(x)+\bar{u}(x)+d(x)+\bar{d}(x)]} + \\
&\quad \frac{D_{d\pi^+}(z)[u(x)+d(x)+4\bar{u}(x)+4\bar{d}(x)]}{5[u(x)+\bar{u}(x)+d(x)+\bar{d}(x)]} \\
&M^{\pi^-}_d(x, Q^2, z) = \\
&\quad \frac{D_{d\pi^-}(z)[4\bar{u}(x)+4\bar{d}(x)+u(x)+d(x)]}{5[u(x)+d(x)+\bar{u}(x)+\bar{d}(x)]} + \\
&\quad \frac{D_{u\pi^-}(z)[\bar{u}(x)+\bar{d}(x)+4u(x)+4d(x)]}{5[u(x)+d(x)+\bar{u}(x)+\bar{d}(x)]},
\end{aligned} \tag{2}$$

where, $D_{u\pi^+}$ and $D_{d\pi^-}$ are the favored FFs and $D_{d\pi^+}$ and $D_{u\pi^-}$ are the un-favored FFs, respectively. Note that under charge symmetry (CS) these reduce to just one favored and one un-favored FF, since CS implies $D_{u\pi^+} = D_{d\pi^-}$. The four FFs as a function of z are extracted from the four multiplicities by simultaneously solving the system of four equations shown above for the eight kinematic settings listed in Table I. These extracted FFs as a function of z are shown in Fig. 8 for the eight kinematic settings. They are also compared to two different global fits of existing data, one by deFlorian, Sassot, and Stratmann (DSS) [6, 7] and the other by the Jefferson Lab Angular Momentum collaboration (JAM) [8]. Within the experimental uncertainties, the four extracted FFs converge to the same values at the lowest x or highest W, over the entire range of z (0.3 - 0.7). At the lowest x or highest W they are also in agreement with the global fits. The FFs deviate from the global fits as x increases or the W decreases. These results likely point to the importance of higher twist corrections at high x or low W kinematics.

A. Systematic Uncertainties

The sources of systematic uncertainties and the total systematic uncertainty of the experiment are listed in Table II. The systematic uncertainty of the charge measurement was determined from the average variation of the charge between data sets collected under similar experimental conditions. The instrumental uncertainty due to electronic noise in the gain monitoring system was also included. There is a 0.7% (0.6%) correlated uncertainty due to uncertainty in the target density for ^{1}H

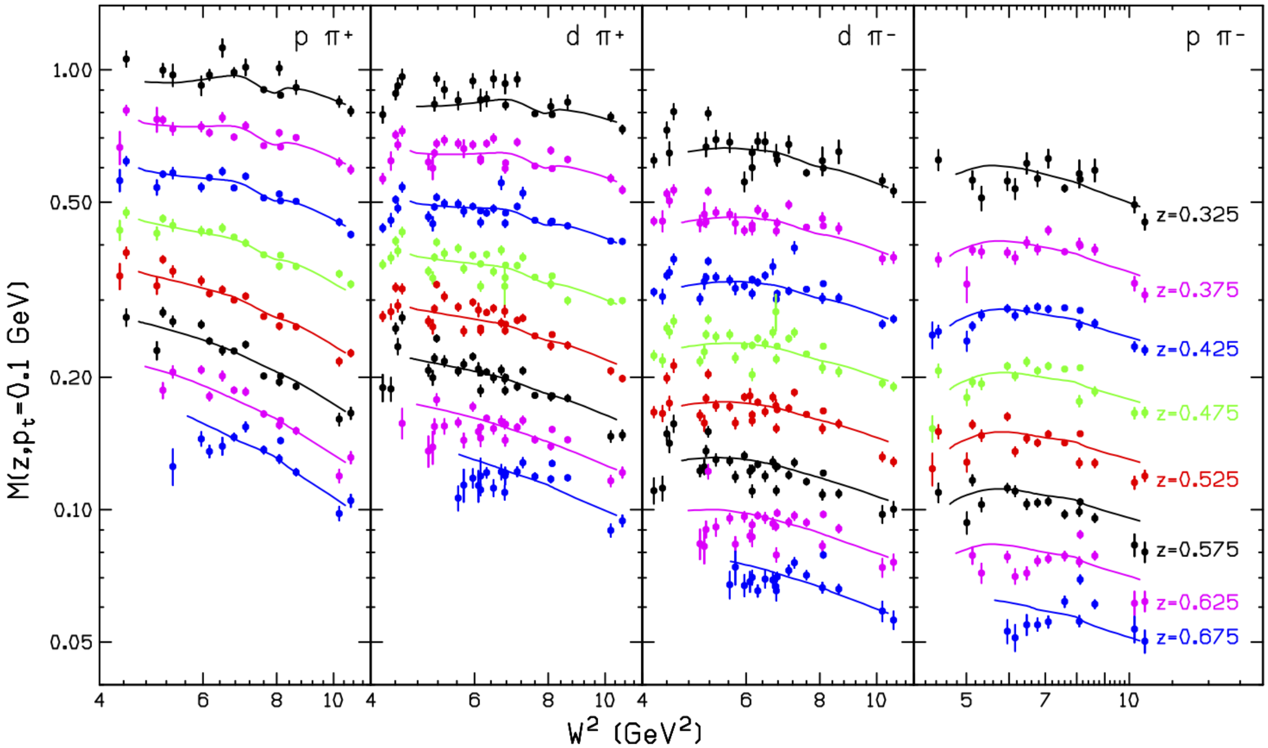

FIG. 7. The multiplicities at $p_T = 0.1$ GeV, averaged over ϕ^* as a function of W^2 for z bins ranging from $z = 0.325$ to 0.675. From left to right, the panels are for π^+ from a proton target, π^+ from a deuteron target, π^- from a deuteron target, and π^- from a proton target, The solid lines are from the empirical fits. Only the statistical uncertainties are shown.

TABLE II. List of systematic uncertainties contributing the uncertainty in the multiplicities/

Source	Uncertainty (%)
Charge	0.45
Target density ^{1}H (^{2}H)	0.7 (0.6)
Target boiling correction	0.2
Target end cap subtraction	0.1
Tracking efficiency	0.1
Live time	0.04
Particle identification	0.8
Background subtraction	< 0.5
Acceptance	0.7
Kinematics	0.1
Radiative correction	1
Inclusive cross-section	2
FADC rate dependence	0.9
Total	2.8

(^{2}H), which includes contributions from the uncertainty in the target length, thermal contraction, temperature, pressure, and the equation of state used to calculate the target density. In addition, the uncertainty in the corrections due to local variation in the cryogenic target density was estimated using dedicated scans of the experimental yield with increasing beam current. These scans were carried out before and after the production period of the experiment. The average variation in the current dependence of the measured yield between multiple scans and multiple equivalent analyses along with the residual current dependence of the yield on a carbon foil was used as the systematic uncertainty for the target boling correction (no current dependent density variation is expected for a carbon foil). The systematic uncertainty due to the tracking efficiency was determined from the average variation of the efficiency between periods with the same trigger rates. The error in the fit parameters of a linear fit of the rate dependence of the live-time correction is used to estimate the systematic uncertainty due to the live-time correction.

The systematic uncertainty in the event selection arising from the particle identification cuts was determined from the average variation in the experimental yield when the cuts were varied by a small fixed amount (typically $\pm10\%$) and between multiple equivalent analyses of the same data set. The systematic uncertainty of the background subtraction procedure arises from the uncertainties in the models used to simulate the various sources of background. This uncertainty was determined from the average variation in the measured yield when the model parameters were varied. The systematic uncertainty due to radiative correction was estimated from the average variation of the correction factor when the generation limits of the simulation of these radiative processes were varied and when the cross section models in the simulation were varied. Additional details on the models of the

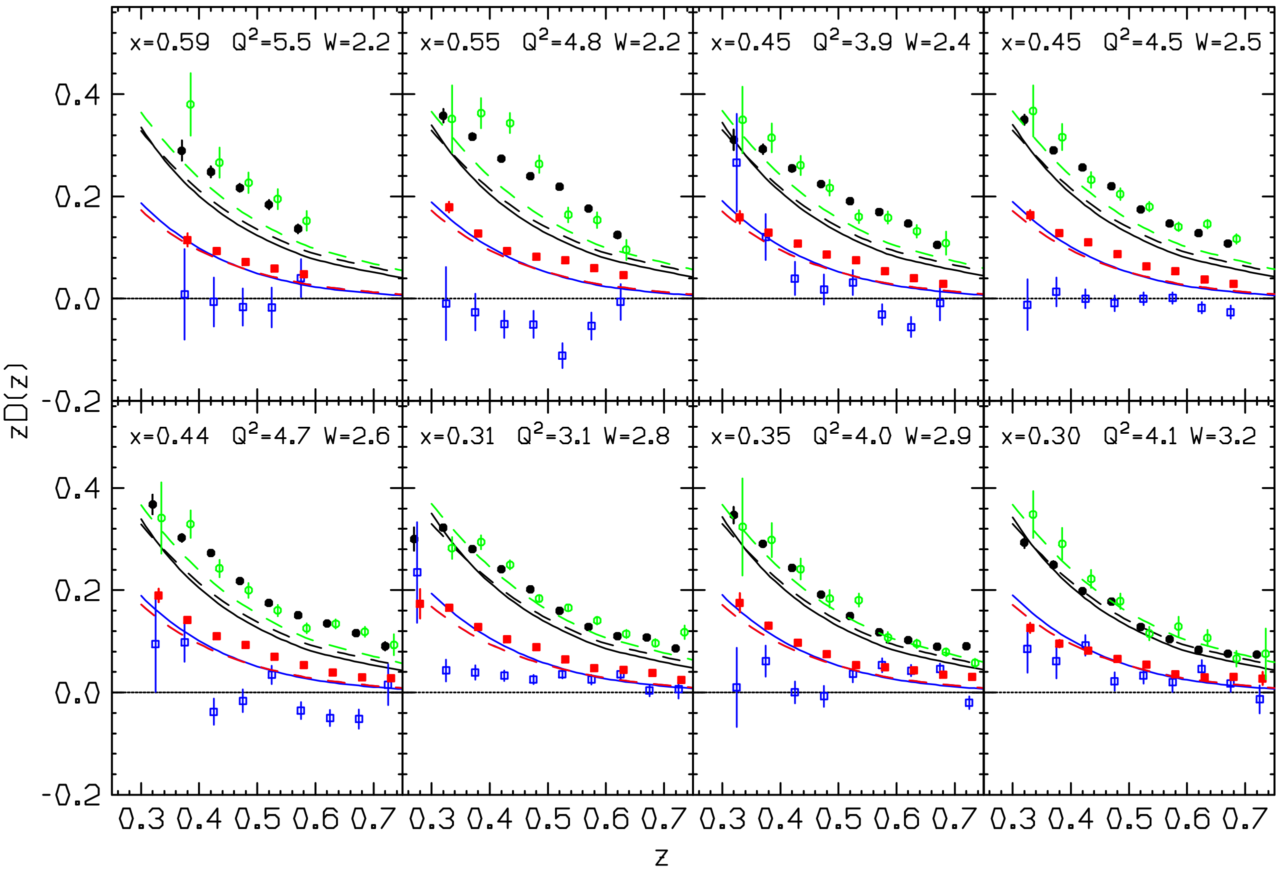

FIG. 8. The 4 extracted FFs shown as a function of z for the eight kinematic settings. The open (green) and solid (black) circles are the two favored FFs while the open (blue) and solid (red) squares are the two unfavored FFs. The dashed lines are the results of global fits from DSS [6, 7], while the solid lines are from the global fit by the JAM collaboration [8]. The JAM collaboration imposes isospin symmetry and hence they produce only one favored FF and one unfavored FF. The error bars show the statistical uncertainties.

radiative processes and their uncertainty can be found in Ref. [9, 10]. The systematic uncertainty due to the acceptance model in the Monte Carlo simulation was estimated from the variation of the multiplicity when the acceptance cuts were varied. The uncertainty due to the beam energy, spectrometer momentum, and angle settings (i.e. kinematic) was determined from the average variation of the multiplicities when the kinematic settings were varied by the measurement uncertainty of the beam energy, spectrometer momentum, and angles. The uncertainty in the inclusive cross section is from the latest fits to the world data [11, 12]. The total systematic uncertainty of 2.8% is the quadrature sum of all uncertainties from the different sources.

For the sum and difference ratios obtained from the multiplicities, most of these systematic uncertainties cancel to first order and were found to be negligible compared to the statistical uncertainty of the sum difference ratios. Only the correlated uncertainty due to target density and the uncertainty due to the inclusive cross section were the major contributions to the sum and difference ratio and led to a 2.2% systematic uncertainty for these ratios. The systematic uncertainty of the extracted FFs arising from the normalization type systematic uncertainties of the multiplicities was studied by scaling the multiplicities and evaluating the variation in the FFs. From this study, the systematic uncertainty of the FFs was determined to be ∼4%. Similarly, the variation in the FF asymmetries was also studied and it was found to be insignificant relative to the larger statistical uncertainty of the asymmetries.

[1] M. Mkrtchyan *et al.*, Nucl. Inst. and Meth. A **719**, 85 (2013).
[2] *The Super High Momentum Spectrometer in Hall-C*, publication in preparation.
[3] M. Mkrtchyan *et al.*, Nucl. Inst. and Meth. A **719**, 85 (2013).

[4] T. Horn *et al.*, Nucl. Inst. and Meth. A **842**, 28 (2017).
[5] `https://coda.jlab.org/drupal/`,.
[6] D. deFlorian, R. Sassot, and M. Stratmann, Phys. Rev. D **75**, 114010 (2007).
[7] D. deFlorian, R. Sassot, M. Epele, R. J. Hernández-Pinto, and M. Stratmann, Phys. Rev. D **91**, 014035 (2015).
[8] E. Moffat, W. Melnitchouk, T. C. Rogers, and N. Sato, Phys. Rev. D **104**, 016015 (2021).
[9] R. Asaturyan *et al.*, Phys. Rev. C **85**, 015202 (2012).
[10] P. Bosted *et al.*, *The P_T and ϕ dependence of the SIDIS cross section*, publication in preparation.
[11] P. E. Bosted and M. E. Christy, Phys. Rev. C **77**, 065206 (2008).
[12] M. E. Christy, Private communication.